On Image Analysis by the Methods of Moments

CHO-HUAK TEH, STUDENT MEMBER, IEEE, AND ROLAND T. CHIN, MEMBER, IEEE

Abstract—**Various types of moments have been used to recognize image patterns in a number of applications. This paper evaluates a number of moments and addresses some fundamental questions, such as image representation ability, noise sensitivity, and information redundancy. Moments considered here include regular moments, Legendre moments, Zernike moments, pseudo-Zernike moments, rotational moments, and complex moments. Properties of these moments are examined in detail and the interrelationships among them are discussed. Both theoretical and experimental results are presented.**

Index Terms—**Image analysis, image reconstruction, image representation, invariance, moment invariants, moments, pattern recognition.**

I. Introduction

MOMENTS and functions of moments have been utilized as pattern features in a number of applications to achieve invariant recognition of two-dimensional image patterns [1]–[9]. Hu [1] first introduced moment invariants in 1961, based on methods of algebraic invariants. Using nonlinear combinations of *regular moments* (regular moments will be referred to as *geometric moments*), he derived a set of invariant moments which has the desirable properties of being invariant under image translation, scaling, and rotation. However, the question of what is gained by including higher order moments in the context of image analysis has not been addressed, and the recovery of the image from these moments is deemed to be quite difficult.

Teague [10] has suggested the notion of orthogonal moments to recover the image from moments based on the theory of orthogonal polynomials, and has introduced *Zernike moments*, which allow independent moment invariants to be constructed easily to an arbitrarily high order. Other orthogonal moments are *Legendre moments*, making use of Legendre polynomials. In [11], *rotational moments* are used to extend the definition of moment invariants to arbitrary order in a manner which ensures that their magnitudes do not diminish significantly with increasing order. More recently, the notion of *complex moments* [12], [13] has been introduced as a simple and straightforward way to derive moment invariants. The definitions of these various types of moments and a summary of their properties are presented in Section II.

Manuscript received June 12, 1986; revised July 29, 1987. Recommended for acceptance by J. Kittler. This work was supported in part by the National Science Foundation under Grant ECS-8352356 and in part by the General Motors Foundation, Inc., Detroit, MI.

The authors are with the Department of Electrical and Computer Engineering, University of Wisconsin, Madison, WI 53706.

IEEE Log Number 8718608.

From the point of view of pattern recognition, moment invariants are considered reliable features if their values are insensitive to the presence of image noise. The effects of sampling, digitizing, and quantization noise on moment invariants have been addressed in [14]. In Section III of this paper, the effect of image noise on various types of moments is analyzed using stochastic images. Second-order statistics of various moments are related to those of the image noise so that the impact of noise can be estimated and compared. In Section IV, information redundancy among different orders of moments is derived for various moment types as an indication of their information content.

It is well known that, in principle, most of the image information can be recaptured by using a sufficiently large number of a particular set of image moments. In Section V, the question of how well an image can be characterized by a small finite set of its moments is investigated by first reconstructing the image from its moments and then evaluating the mean-square reconstruction error. Theoretical results for stochastic images under both noise-free and noisy conditions are derived. The error is expressed as a function of the statistical properties of the image function and the noise process. Experimental results for a set of chosen test images are also presented.

II. Moments

In this section, the various types of moments are defined and their properties briefly summarized. We assume that the real image intensity function $f(x, y)$ is piecewise continuous and has bounded support.

A. Geometric Moments (GM)

The geometric moments of order $(p + q)$ of $f(x, y)$ are defined as

$$M_{pq} = \int_{-\infty}^{\infty} \int_{-\infty}^{\infty} x^p y^q f(x, y)\, dx\, dy \qquad (2.1)$$

where $p, q = 0, 1, 2, \cdots, \infty$. The above definition has the form of the projection of the function $f(x, y)$ onto the monomial $x^p y^q$. However, the basis set $\{x^p y^q\}$, while complete (Weierstrass approximation theorem [15]), is not orthogonal.

B. Legendre Moments (LM)

The Legendre moments of order $(m + n)$ are defined as

$$\lambda_{mn} = \frac{(2m+1)(2n+1)}{4} \cdot \int_{-\infty}^{\infty}\int_{-\infty}^{\infty} P_m(x)\,P_n(y)\,f(x,y)\,dx\,dy \quad (2.2)$$

where $m, n = 0, 1, 2, \cdots, \infty$. The Legendre polynomials $\{P_m(x)\}$ [15] are a complete orthogonal basis set on the interval $[-1, 1]$:

$$\int_{-1}^{1} P_m(x)\,P_n(x) = \frac{2}{2m+1}\,\delta_{mn}. \quad (2.3)$$

The nth-order Legendre polynomial is

$$P_n(x) = \sum_{j=0}^{n} a_{nj}x^j = \frac{1}{2^n n!}\frac{d^n}{dx^n}(x^2-1)^n. \quad (2.4)$$

By the orthogonality principle, the image function $f(x, y)$ can be written as an infinite series expansion in terms of the Legendre polynomials over the square $[-1 \le x, y \le 1]$:

$$f(x,y) = \sum_{m=0}^{\infty}\sum_{n=0}^{\infty} \lambda_{mn}P_m(x)\,P_n(y) \quad (2.5)$$

where the Legendre moments $\{\lambda_{mn}\}$ are computed over the same square. If only Legendre moments of order $\le N$ are given, then the function $f(x, y)$ can be approximated by a continuous function which is a truncated series:

$$f(x,y) \approx \sum_{m=0}^{N}\sum_{n=0}^{m} \lambda_{m-n,n}P_{m-n}(x)\,P_n(y). \quad (2.6)$$

Using (2.1), (2.2), and (2.4), the Legendre moments and geometric moments are related by

$$\lambda_{mn} = \frac{(2m+1)(2n+1)}{4}\sum_{j=0}^{m}\sum_{k=0}^{n} a_{mj}a_{nk}M_{jk}. \quad (2.7)$$

Thus, a given Legendre moment depends only on geometric moments of the same order and lower, and conversely.

C. Zernike Moments (ZM)

The complex Zernike moments of order n with repetition l are defined as

$$A_{nl} = \frac{n+1}{\pi}\int_0^{2\pi}\int_0^{\infty} [V_{nl}(r,\theta)]^* \cdot f(r\cos\theta, r\sin\theta)\,r\,dr\,d\theta \quad (2.8)$$

where $n = 0, 1, 2, \cdots, \infty$ and l takes on positive and negative integer values subject to the conditions

$$n - |l| = \text{even}, \qquad |l| \le n. \quad (2.9)$$

The symbol * denotes the complex conjugate. The Zernike polynomials [16]

$$v_{nl}(x,y) = V_{nl}(r\cos\theta, r\sin\theta) = R_{nl}(r)\,e^{il\theta} \quad (2.10)$$

are a complete set of complex-valued functions orthogonal on the unit disk $x^2 + y^2 \le 1$:

$$\int_0^{2\pi}\int_0^{1} [V_{nl}(r,\theta)]^* V_{mk}(r,\theta)\,r\,dr\,d\theta = \frac{\pi}{n+1}\,\delta_{mn}\delta_{kl}. \quad (2.11)$$

The real-valued radial polynomials $\{R_{nl}(r)\}$ satisfy the relations

$$\int_0^1 R_{nl}(r)\,R_{ml}(r)\,r\,dr = \frac{1}{2(n+1)}\,\delta_{mn} \quad (2.12)$$

and are defined as

$$R_{nl}(r) = \sum_{s=0}^{(n-|l|)/2} (-1)^s \cdot \frac{(n-s)!}{s!\left(\frac{n+|l|}{2}-s\right)!\left(\frac{n-|l|}{2}-s\right)!}\,r^{n-2s} = \sum_{\substack{k=|l| \\ n-k=\text{even}}}^{n} B_{n|l|k}r^k. \quad (2.13)$$

The function $f(x, y)$ can be expanded in terms of the Zernike polynomials over the unit disk as

$$f(x,y) = \sum_{n=0}^{\infty}\sum_{\substack{l=-\infty \\ n-|l|=\text{even} \\ |l|\le n}}^{\infty} A_{nl}V_{nl}(x,y) \quad (2.14)$$

where the Zernike moments $\{A_{nl}\}$ are computed over the unit disk. If the series expansion is truncated at a finite order N, then the truncated expansion is the optimum approximation to $f(x, y)$:

$$f(x,y) \approx \sum_{n=0}^{N}\sum_{\substack{l \\ n-|l|=\text{even} \\ |l|\le n}} A_{nl}V_{nl}(x,y). \quad (2.15)$$

Note that because of the orthogonality of the Legendre and Zernike polynomials, both the Legendre moments $\{\lambda_{mn}\}$ in (2.5) and the Zernike moments $\{A_{nl}\}$ in (2.14) are in each case independent. It can be shown that Zernike moments and geometric moments are related by

$$A_{nl} = \frac{n+1}{\pi}\sum_{\substack{k=|l| \\ n-k=\text{even}}}^{n}\sum_{j=0}^{q}\sum_{m=0}^{|l|} w^m \cdot \binom{q}{j}\binom{|l|}{m} B_{n|l|k}M_{k-2j-m,2j+m} \quad (2.16)$$

where

$$w = \begin{cases} -i & l > 0 \\ +i & l \le 0, \end{cases} \quad (2.17)$$

$q = \frac{1}{2}(k - |l|)$, and $i = \sqrt{-1}$.

D. Pseudo-Zernike Moments (PM)

Zernike polynomials were first introduced in 1934 [17] and were later derived from the requirement of orthogo-

nality and invariance properties by Bhatia and Wolf [18]. Zernike polynomials, being invariant in form with respect to rotations of axis about the origin, are polynomials in x and y. A related orthogonal set of polynomials in x, y, and r was derived in [18] which has properties analogous to those of Zernike polynomials. This set of polynomials, which we shall call pseudo-Zernike polynomials, differs from that of Zernike in that the real-valued radial polynomials are defined as

$$R_{nl}(r) = \sum_{s=0}^{n-|l|} (-1)^s \cdot \frac{(2n+1-s)!}{s!(n-|l|-s)!(n+|l|+1-s)!} r^{n-s} = \sum_{k=|l|}^{n} S_{n|l|k} r^k \tag{2.18}$$

where now $n = 0, 1, 2, \cdots, \infty$ and l takes on positive and negative integer values subject to $|l| \leq n$ only. By simple enumeration, this set of pseudo-Zernike polynomials contains $(n+1)^2$ linearly independent polynomials of degree $\leq n$, whereas the set of Zernike polynomials contains only $\frac{1}{2}(n+1)(n+2)$ linearly independent polynomials of degree $\leq n$ due to the additional condition of $n - |l| =$ even.

The Zernike moments in (2.8) become pseudo-Zernike moments if the radial polynomials $\{R_{nl}(r)\}$ in (2.18), which also satisfy the relations in (2.12), are used to compute the polynomials with the condition $n - |l| =$ even eliminated. Since the pseudo-Zernike polynomials are also a complete set of functions orthogonal on the unit disk, both the series expansions of $f(x, y)$ in (2.14) and (2.15) hold with the condition $n - |l| =$ even eliminated, and $\{A_{nl}\}$ and $\{V_{nl}(x, y)\}$ are now the pseudo-Zernike moments and the pseudo-Zernike polynomials, respectively. In addition, the pseudo-Zernike moments are independent. It is shown in Section III that pseudo-Zernike moments are less sensitive to image noise than are the conventional Zernike moments.

E. Rotational Moments (RM)

The rotational moments of order n with repetition l are defined as

$$D_{nl} = \int_0^{2\pi} \int_0^{\infty} r^n e^{-il\theta} f(r\cos\theta, r\sin\theta) r\, dr\, d\theta \tag{2.19}$$

where $n = 0, 1, 2, \cdots, \infty$ and l takes on any positive and negative integer values. From (2.8), (2.10), (2.13), and (2.19), it can be shown that Zernike moments and rotational moments are related by

$$A_{nl} = \frac{n+1}{\pi} \sum_{\substack{k=|l| \\ n-k=\text{even}}}^{n} B_{n|l|k} D_{kl} \tag{2.20}$$

from which it follows that rotational moments can also be obtained from geometric moments by

$$D_{nl} = \sum_{j=0}^{q} \sum_{m=0}^{|l|} w^m \binom{q}{j} \binom{|l|}{m} M_{n-2j-m,2j+m} \tag{2.21}$$

where w is given by (2.17) and $q = \frac{1}{2}(n - |l|)$. Unlike Legendre and Zernike moments, the rotational moments $\{D_{nl}\}$ are not generally independent.

F. Complex Moments (CM)

The notion of complex moments was recently introduced in [12] as a simple and straightforward way to derive moment invariants. The complex moments of order $(p+q)$ are defined as

$$C_{pq} = \int_{-\infty}^{\infty} \int_{-\infty}^{\infty} (x+iy)^p (x-iy)^q f(x, y)\, dx\, dy \tag{2.22}$$

where $p, q = 0, 1, 2, \cdots, \infty$, and $i = \sqrt{-1}$. The complex moment of order $(p+q)$ is a linear combination with complex coefficients of the geometric moments $\{M_{rs}\}$ satisfying $r + s = p + q$:

$$C_{pq} = \sum_{r=0}^{p} \sum_{s=0}^{q} \binom{p}{r} \binom{q}{s} i^{p+q-(r+s)} \cdot (-1)^{q-s} M_{r+s,p+q-(r+s)}. \tag{2.23}$$

In polar coordinates, the complex moment of order $(p+q)$ can be written as

$$C_{pq} = \int_0^{2\pi} \int_0^{\infty} r^{p+q} e^{i(p-q)\theta} f(r\cos\theta, r\sin\theta) r\, dr\, d\theta; \tag{2.24}$$

thus, it is related to the rotational moments as

$$D_{nl} = C_{1/2(n-l),1/2(n+l)}, \tag{2.25}$$

from which it also follows that Zernike moments and complex moments are related by

$$A_{nl} = \frac{n+1}{\pi} \sum_{\substack{k=|l| \\ n-k=\text{even}}}^{n} B_{n|l|k} C_{1/2(k-l),1/2(k+l)}. \tag{2.26}$$

From (2.24), the repetition of C_{pq} is defined as $p - q$. Like the rotational moments, the complex moments $\{C_{pq}\}$ are not independent.

III. Noise Sensitivity

Moment invariants using various schemes [2], [8]–[11] based on the different moment types as defined in the previous section have been shown to provide perfect invariance properties under noise-free condition. However, in the presence of noise, the computed invariant moments are expected not to be strictly invariant. Thus, it is important to investigate which invariance scheme is less vulnerable to image noise. In this section, the various types of moments, and hence their corresponding moment invariants, of noisy images are analyzed and compared. Theoretical expressions relating the second-order statis-

tics of the various types of moments and those of additive noise are derived to estimate the impact of noise.

In the following, we assume that $f(x, y)$ is a real homogeneous (i.e., wide-sense stationary) random field defined over a region ζ of the xy plane, and for convenience, we assume that the random field $f(x, y)$ has zero mean:

$$E\{f(x, y)\} = 0 \tag{3.1}$$

where the operation of expectation is ensemble averaging. Experimental evidence [19]–[21] indicates that a reasonable autocorrelation function for $f(x, y)$ is of the form

$$K_{ff}(x, y, u, v) = K_{ff}(0, 0)\, e^{-c_1|x-u| - c_2|y-v|} \tag{3.2}$$

where c_1 and c_2 are positive constants and

$$K_{ff}(0, 0) = E\{[f(x, y)]^2\} \tag{3.3}$$

is the average energy of the random field. By choosing different values for c_1 and c_2, the above autocorrelation function can be used to model images with different amounts of correlation in the horizontal and vertical directions. In general, the greater amounts of detail in the image, the larger the values of c_1 and c_2 that should be chosen. We also assume that the noise process $n(x, y)$ is of zero mean and is white with autocorrelation function

$$K_{nn}(x, y, u, v) = \sigma_n^2 \delta(x - u, y - v) \tag{3.4}$$

where $\delta(x - u, y - v)$ is the two-dimensional Delta function and σ_n^2 is the two-dimensional spectral density of the noise process.

It is noted that each of the moment sets defined in the previous section has the following general form:

$$\Phi_{pq} = \iint_{\zeta} \phi_{pq}(x, y)\, f(x, y)\, dx\, dy \tag{3.5}$$

where $\phi_{pq}(x, y)$ is the moment weighting kernel (i.e., $\{\phi_{pq}(x, y)\}$ is the basis set) and Φ_{pq} is the moment of order (p, q) of $f(x, y)$. The moment of order (p, q) of the noise process $n(x, y)$ can be defined in a similar form as

$$N_{pq} = \iint_{\zeta} \phi_{pq}(x, y)\, n(x, y)\, dx\, dy. \tag{3.6}$$

Note that both Φ_{pq} and N_{pq} are zero-mean random variables. The covariance of any two moments of the noise process can be expressed as

$$\begin{aligned} \operatorname{cov}\{N_{pq}, N_{rs}\} &= E\{N_{pq} N_{rs}^*\} \\ &= \iint_{\zeta}\iint_{\zeta} \phi_{pq}(x, y)\, \phi_{rs}(x, y) \\ &\quad \cdot K_{nn}(x, y, u, v)\, dx\, dy\, du\, dv. \end{aligned} \tag{3.7}$$

In order to evaluate the effect of noise on moments of different orders and to compare how various types of moments are affected by noise, we define the unnormalized and normalized signal-to-noise ratios of order (p, q) as

$$\mathrm{SNR}_{pq} = \frac{\operatorname{var}\{\Phi_{pq}\}}{\operatorname{var}\{N_{pq}\}} \tag{3.8}$$

and

$$\overline{\mathrm{SNR}}_{pq} = \mathrm{SNR}_{pq} \frac{\sigma_n^2}{K_{ff}(0, 0)} \tag{3.9}$$

where $\operatorname{var}\{\Phi_{pq}\}$ and $\operatorname{var}\{N_{pq}\}$ are the variances of Φ_{pq} and N_{pq}, respectively. For computational and comparison purposes, we take the random field to vanish outside the square $[-1 \le x, y \le 1]$. The SNR's for different moment sets are evaluated and listed in Table I.

The following observations follow from Table I.

1) The radial polynomials $\{R_{nl}(r)\}$ in (2.13) depend only on the absolute values of repetitions (l). Thus, Zernike moments A_{nl} and $A_{n,-l}$ have the same SNR's. This is also true for pseudo-Zernike moments, rotational moments, and complex moments.

2) A_{nn} (both Zernike and pseudo-Zernike moments) and D_{nn} have the same SNR's since $R_{nn}(r) = r^n$ (for both Zernike and pseudo-Zernike polynomials).

3) Rotational and complex moments of the same order and with zero repetition have the same SNR's. In this case, n = even and $l = 0$ for rotational moments, $p = q$ for complex moments, and $n = p + q = 2p$ for rotational moments and complex moments.

4) C_{pq} and C_{qp} have the same SNR's since $C_{pq} = C_{qp}^*$ for a real image function.

5) If the random field $f(x, y)$ has equal correlation in the horizontal and vertical directions, i.e., $c_1 = c_2$ in (3.2), then M_{pq} and M_{qp} have the same SNR's, which is also true for λ_{mn} and λ_{nm}.

For illustration purposes, we choose $c_1 = c_2 = 1$. Based on the above observations, the $\overline{\mathrm{SNR}}$'s as defined in (3.9) are plotted for

1) $\{M_{pp}, \lambda_{pp}, C_{pp}, p = 0, 1, 2, \cdots, 13; A_{nn}, n = 0, 2, 4, \cdots, 26\}$ in Fig. 1, and

2) $\{A_{nl}$ for both ZM and PM, $D_{nl}, n = 0, 1, 2, \cdots, 13; l = 0$ for n = even and $l = 1$ for n = odd$\}$ in Fig. 2.

Both figures show the general trend that higher order moments are more sensitive to image noise than are lower order moments. In addition, Fig. 1 shows that complex moments of a particular order are slightly less affected by noise than are geometric moments of the same order, and Legendre moments are more severely affected by noise than the rest of the moments. Fig. 2 shows that pseudo-Zernike moments are less affected by noise than are rotational and Zernike moments.

It is clear from both figures that higher order moments are more vulnerable to white noise. This makes their use undesirable in image representation and pattern recognition. On the other hand, it is shown in Section V that only moments of higher orders carry the fine detail of an image. These two conflicting factors generally put a limit on

TABLE I
COMPARISON OF THE SIGNAL-TO-NOISE RATIOS FOR DIFFERENT MOMENT SETS

Type of Moment		Signal-to-Noise Ratio SNR_{pq}
GM	M_{pq}	$\frac{(2p+1)(2q+1)}{4\sigma_n^2}\int\int\int\int (xu)^p (yv)^q K_{ff}(x, y, u, v)\, dx\, dy\, du\, dv$
LM	λ_{mn}	$\frac{(2m+1)(2n+1)}{4\sigma_n^2}\int\int\int\int P_m(x)\, P_m(u)\, P_n(y)\, P_n(v)\, K_{ff}(x, y, u, v)\, dx\, dy\, du\, dv$
ZM, PM	A_{nl}	$\frac{\int\int\int\int R_{nl}(r)\, R_{nl}(\rho)\cos[l(\theta-\phi)] K_{ff}(x, y, u, v)\, dx\, dy\, du\, dv}{\sigma_n^2 \int\int [R_{nl}(r)]^2\, dx\, dy}$
RM	D_{nl}	$\frac{\int\int\int\int (r\rho)^n \cos[l(\theta-\phi)] K_{ff}(x, y, u, v)\, dx\, dy\, du\, dv}{\sigma_n^2 \int\int r^{2n}\, dx\, dy}$
CM	C_{pq}	$\frac{\int\int\int\int (r\rho)^{p+q} \cos[(p-q)(\theta-\phi)] K_{ff}(x, y, u, v)\, dx\, dy\, du\, dv}{\sigma_n^2 \int\int r^{2(p+q)}\, dx\, dy}$

All the integration limits are from -1 to 1.
$x = r\cos(\theta)$, $y = r\sin(\theta)$.
$u = \rho\cos(\phi)$, $v = \rho\sin(\phi)$.

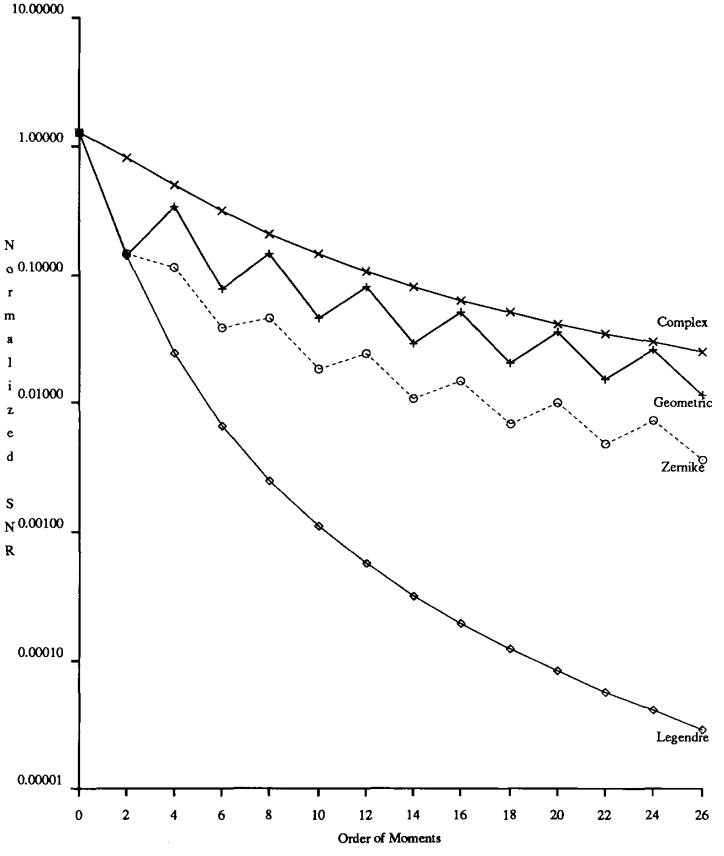

Fig. 1. Comparison of the normalized signal-to-noise ratios for different moment sets ($c_1 = c_2 = 1$) (lines connecting data points are for illustration purposes and y axis is in log scale).

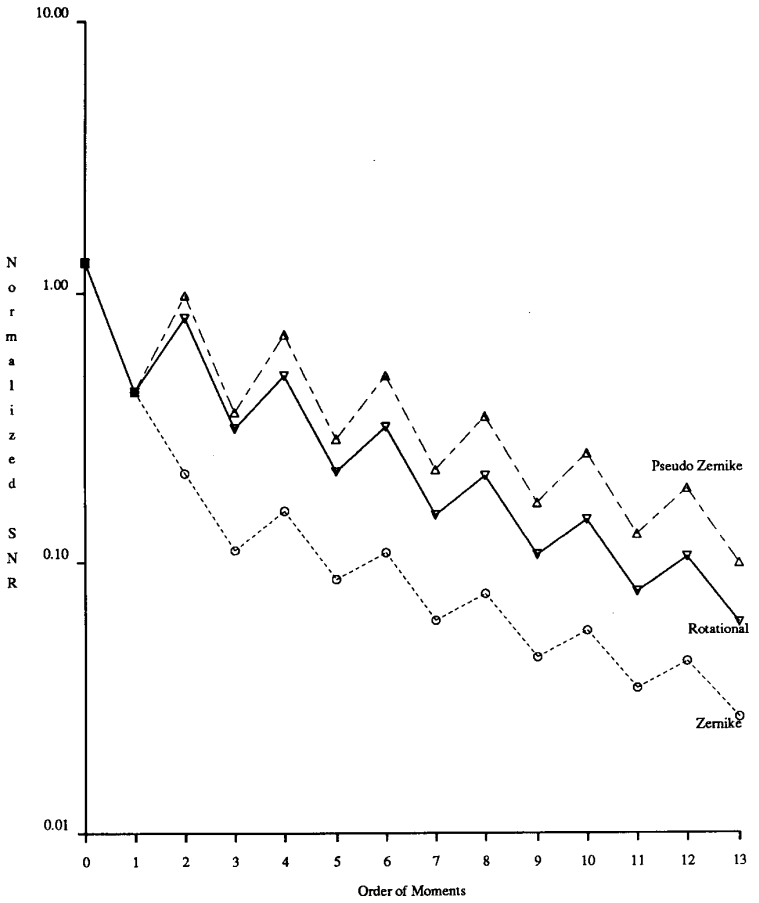

Fig. 2. Comparison of the normalized signal-to-noise ratios for different moment sets ($c_1 = c_2 = 1$) (lines connecting data points are for illustration purposes and y axis is in log scale).

the optimal number of moments which are useful in any given problem. This fact is demonstrated in Section V, in which for a specific noise level, an image is best characterized by using moments of up to certain high orders.

IV. Information Redundancy

Of the various moment types defined in Section II, only the Legendre, Zernike, and pseudo-Zernike moments are orthogonal. This implies that except for the LM, ZM, and PM kernels, the moment weighting kernels are correlated. Correlation between kernels is directly related to information-theoretic redundancy [12] showing how informative the moments are. In this section, the redundancy properties of geometric, rotational, and complex moments are investigated through their connections with Legendre and Zernike moments. To make the analysis feasible, a zero-mean, unit variance white noise process $\boldsymbol{n}(x, y)$ is used instead of $\boldsymbol{f}(x, y)$ for moment calculations. The analysis for the case of $\boldsymbol{f}(x, y)$, with autocorrelation function of the form given by (3.2), can be shown to lead to the same results. The covariance of any two moments of the noise process as defined in (3.7) is evaluated over the appropriate region for various moment types; the results are listed in Table II.

Table II shows that Legendre, Zernike, and pseudo-Zernike moments are uncorrelated moment sets, whereas only those geometric moments with the special conditions of $p + r =$ odd or $q + s =$ odd are uncorrelated. In the cases of rotational and complex moments, only those with the same repetition ($l = k$ for RM and $p - q = r - s$ for CM) are respectively correlated, which are also respectively statistically in phase. It is also noted that the variance of Zernike, pseudo-Zernike, rotational, and complex moments of the noise process depends only on the order and not on the repetition.

A. Information Redundancy of Rotational and Complex Moments

Zernike and rotational moments are related by (2.20), which we rewrite here for convenience:

$$A_{nl} = \frac{n+1}{\pi} \sum_{\substack{k=|l| \\ n-k=\text{even}}}^{n} B_{n|l|k} D_{kl}. \tag{4.1}$$

Note that for a given repetition l, the rotational moments

TABLE II
COVARIANCE OF MOMENTS OF WHITE NOISE PROCESS FOR DIFFERENT MOMENT SETS

Type of Moment		Region of Integration	cov $\{N_{pq}, N_{rs}\}$, Assuming $\sigma_n^2 = 1$
GM	M_{pq}	Square $[-1 \le x, y \le 1]$	$\text{cov}\{N_{pq}, N_{rs}\} = \frac{[1-(-1)^{p+r+1}][1-(-1)^{q+s+1}]}{(p+r+1)(q+s+1)}$
LM	λ_{mn}	Square $[-1 \le x, y \le 1]$	$\text{cov}\{N_{mn}, N_{rs}\} = \frac{(2m+1)(2n+1)}{4}\delta_{mr}\delta_{ns}$
ZM, PM	A_{nl}	Unit Disk	$\text{cov}\{N_{nl}, N_{mk}\} = \frac{n+1}{\pi}\delta_{mn}\delta_{lk}$
RM	D_{nl}	Unit Disk	$\text{cov}\{N_{nl}, N_{mk}\} = \frac{2\pi}{n+m+2}\delta_{lk}$
CM	C_{pq}	Unit Disk	$\text{cov}\{N_{pq}, N_{rs}\} = \frac{2\pi}{p+q+r+s+2}\delta_{p-q,r-s}$

$\{D_{kl}\}$ have the same repetition, and hence are correlated. If Zernike moments of order $\le 2N$, $\{A_{nl}, n = |l|, |l|+2, \cdots, 2N\}$ are given, then the set of rotational moments $\{D_{kl}, k = |l|, |l|+2, \cdots, 2N\}$ can be obtained recursively by

$$D_{kl} = \frac{\pi}{(k+1)B_{k|l|k}} A_{kl} - \sum_{\substack{j=|l| \\ k-j=\text{even}}}^{k-2} \frac{B_{k|l|j}}{B_{k|l|k}} D_{jl}, \quad k = |l|+2, |l|+4, \cdots, 2N \tag{4.2}$$

with

$$D_{|l|l} = \frac{\pi}{(|l|+1)B_{|l||l||l|}} A_{|l|l}. \tag{4.3}$$

The second term in (4.2) is actually a function of all Zernike moments of order $\le k-2$ with repetition l. Thus, (4.2) can be rewritten as

$$D_{kl} = \frac{\pi}{(k+1)B_{k|l|k}} A_{kl} - \sum_{\substack{n=|l| \\ k-n=\text{even}}}^{k-2} \alpha_n A_{nl}, \quad k = |l|+2, |l|+4, \cdots, 2N \tag{4.4}$$

where the coefficient $\{\alpha_n\}$, which is a function of $\{B_{n|l|k}\}$, can be determined easily from (4.2) and (4.3). The rotational moment D_{kl} in (4.4) can be viewed as consisting of two components; the first component (the second term) contains information which is already contained in the rotational moment $D_{k-2,l}$, and the second component (the first term) contains new information which is uncorrelated with the first component. In terms of information redundancy, the first component is redundant. We define the ratio between the informative part and the redundant part as

$$\gamma(k) = \frac{\text{var}\left\{\frac{\pi}{(k+1)B_{k|l|k}} A_{kl}\right\}}{\text{var}\left\{-\sum_{\substack{n=|l| \\ k-n=\text{even}}}^{k-2} \alpha_n A_{nl}\right\}}, \quad k = |l|+2, |l|+4, \cdots, 2N \tag{4.5}$$

where var $\{A_{kl}\}$ is the variance of the Zernike moment A_{kl} of the process. In the case of a zero-mean, unit variance, white noise process $n(x, y)$, we have from Table II,

$$\text{var}\{A_{kl}\} = \frac{k+1}{\pi}. \tag{4.6}$$

The ratio $\gamma(k)$ is plotted in Fig. 3 for the case of $l = 0$ and $k = 2, 4, \cdots, 20$. Notice how this ratio becomes very small for large values of k. This implies that the information contained in the rotational moment D_{kl}, which is already provided by $D_{k-2,l}$, dominates the new information.

For complex moments, we have from (2.26) for a given repetition l,

$$A_{nl} = \frac{n+1}{\pi} \sum_{\substack{k=|l| \\ n-k=\text{even}}}^{n} B_{n|l|k} C_{1/2(k-l),1/2(k+l)} \tag{4.7}$$

where $n = |l|, |l|+2, \cdots, \infty$. The complex moments $\{C_{1/2(k-l),1/2(k+l)}\}$ have the same repetition, and hence are correlated. But from (2.25),

$$C_{1/2(k-l),1/2(k+l)} = D_{kl}; \tag{4.8}$$

thus, we get the same results as in the case of rotational moments.

B. Information Redundancy of Geometric Moments

Let us consider the case of $m = 0$ and $n =$ even in (2.7); then

$$\lambda_{0n} = \frac{(2n+1)}{4} \sum_{\substack{k=0 \\ k=\text{even}}}^{n} a_{nk} M_{0k}. \tag{4.9}$$

In this case, the geometric moments $\{M_{0k}\}$ are correlated. Given $\{\lambda_{0n}, n = 0, 2, \cdots, 2N\}$, $\{M_{0k}, k = 0, 2, \cdots, 2N\}$ can be expressed as

$$M_{0k} = \sum_{\substack{n=0 \\ n=\text{even}}}^{k} \beta_n \lambda_{0n} \tag{4.10}$$

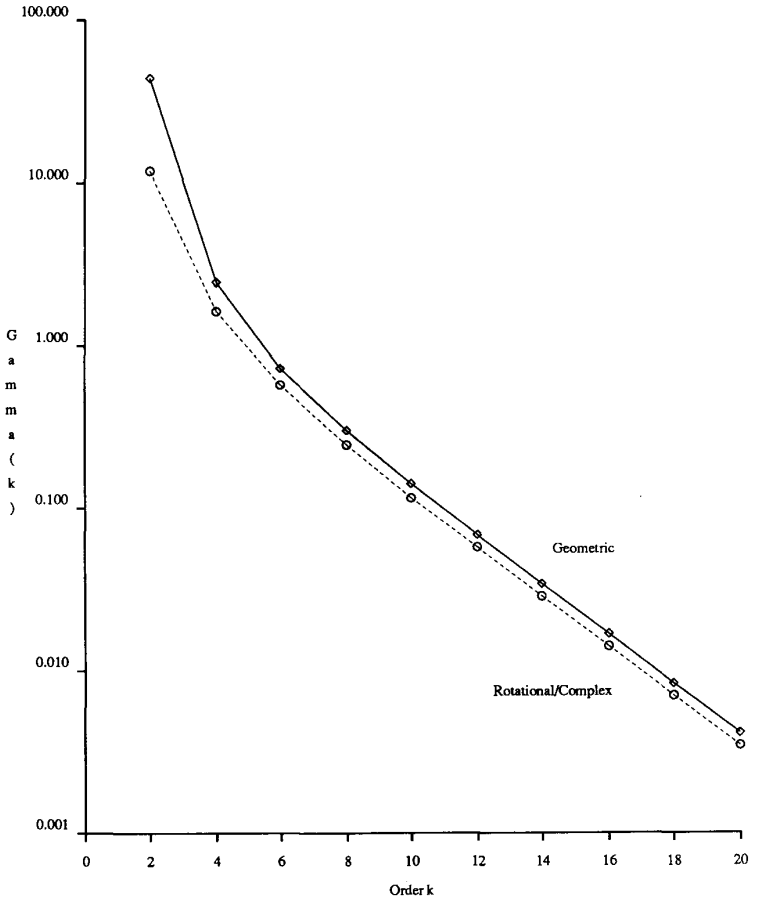

Fig. 3. Illustration of information redundancy of rotational and complex moments and geometric moments (lines connecting data points are for illustration purposes and y axis is in log scale).

where the coefficient $\{\beta_n\}$ is a function of $\{a_{nk}\}$. Now the ratio between the informative part and the redundant part is defined as

$$\gamma(k) = \frac{\text{var}\{\beta_k \lambda_{0k}\}}{\text{var}\left\{\sum_{\substack{n=0 \\ n=\text{even}}}^{k-2} \beta_n \lambda_{0n}\right\}}, \quad k = 2, 4, \cdots, 2N \tag{4.11}$$

where from Table II,

$$\text{var}\{\lambda_{0k}\} = \frac{2k+1}{4}. \tag{4.12}$$

The ratio $\gamma(k)$ is plotted in Fig. 3 for $k = 2, 4, \cdots, 20$, from which it is observed that geometric moments have information redundancy similar to that of rotational moments.

V. Image Representation by Moments

In this section, the question of how well an image can be characterized by a small finite set of its moments is addressed. The mean-square error between an image and its reconstructed version from a finite set of its moments is considered to be a good measure of the image representation ability of the moments. This mean-square reconstruction error measure is applied to both deterministic image functions and real homogeneous random fields to determine the dependence of the accuracy of reconstruction on the number of moments used for the representation. Through this investigation, the information content of higher order moments becomes apparent.

A. Reconstruction Error of Deterministic Image Functions

Let $f(x, y)$ be a deterministic image function defined over a region ζ of the xy plane and let $\hat{f}(x, y)$ be the reconstructed version of $f(x, y)$ when moments of order $\leq N$ are used to characterize the image function. Then the mean-square reconstruction error is defined as

$$e^2(N) = \iint_{\zeta} [f(x, y) - \hat{f}(x, y)]^2 \, dx \, dy. \tag{5.1}$$

For convenience of performance comparison, we normalized $e^2(N)$ by the total image energy and define the nor-

malized reconstruction error as

$$\bar{e}^2(N) = \frac{e^2(N)}{\iint_{\zeta} [f(x, y)]^2 \, dx \, dy}. \tag{5.2}$$

Note that

$$0 \le \bar{e}^2(N) \le 1. \tag{5.3}$$

For the case of discrete data processing, (5.2) becomes

$$\bar{e}^2(N) = \frac{\sum_i \sum_j [f(i, j) - \hat{f}(i, j)]^2}{\sum_i \sum_j [f(i, j)]^2}. \tag{5.4}$$

By substituting (2.6) and (2.15) into (5.1), the reconstruction errors when Legendre and Zernike moments of order $\le N$ are used to characterize the original image function are evaluated to be

$$e_L^2(N) = \int_{-1}^{1} \int_{-1}^{1} [f(x, y)]^2 \, dx \, dy - \sum_{m=0}^{N} \sum_{n=0}^{m} \frac{4\lambda_{mn}^2}{(2m - 2n + 1)(2n + 1)} \tag{5.5}$$

and

$$e_Z^2(N) = \int_0^{2\pi} \int_0^1 [f(r, \theta)]^2 r \, dr \, d\theta - \sum_{n=0}^{N} \sum_{\substack{l \\ n - |l| = \text{even} \\ |l| \le n}} \frac{\pi}{n + 1} |A_{nl}|^2, \tag{5.6}$$

respectively, where $\{\lambda_{mn}\}$ and $\{A_{nl}\}$ are the respective moment sets. By simple enumeration, the number of independent moments in each of the above moment sets is the same and is equal to

$$N_{\text{total}} = \frac{(N + 1)(N + 2)}{2}. \tag{5.7}$$

For the case of pseudo-Zernike moments, the reconstruction error is given by (5.6) with the condition $n - |l| =$ even eliminated, and the set $\{A_{nl}\}$ which is now pseudo-Zernike moments of order $\le N$ is computed as described in Section II-D. The number of independent moments in the set $\{A_{nl}\}$ is equal to

$$N_{\text{total}} = (N + 1)^2. \tag{5.8}$$

For the case of nonorthogonal moments, which includes geometric, rotational, and complex moments, the reconstruction errors can be obtained from (5.5) and (5.6) through their connections with Legendre and Zernike moments. If moments of order $\le N$ are used to characterize the image function, the reconstruction errors of nonorthogonal moments can be shown to be equal to those of Legendre moments and Zernike moments with the image function being restricted to the square $[-1 \le x, y \le 1]$ and the unit disk, respectively.

B. Reconstruction Error of Homogeneous Random Fields

When $f(x, y)$ is a real homogeneous random field, the mean-square reconstruction error when averaged over the random field is defined as

$$\varepsilon^2(N) = E\left\{ \iint_{\zeta} [f(x, y) - \hat{f}(x, y)]^2 \, dx \, dy \right\} \tag{5.9}$$

$$= E\{e^2(N)\} \tag{5.10}$$

and its normalized version as

$$\bar{\varepsilon}^2(N) = \frac{\varepsilon^2(N)}{E\left\{ \iint_{\zeta} [f(x, y)]^2 \, dx \, dy \right\}} \tag{5.11}$$

$$= \frac{\varepsilon^2(N)}{AK_{ff}(0, 0)} \tag{5.12}$$

where we again assume that the random field is of zero mean with the autocorrelation function of the form given by (3.2) and A is the area of the region ζ. Note that $e_L^2(N)$ and $\{\lambda_{mn}\}$ of (5.5) and $e_Z^2(N)$ and $\{A_{nl}\}$ of (5.6) are interpreted as random variables when they are substituted into (5.10).

Using (5.10), (5.5), and (5.6) and the definitions of Legendre and Zernike moments, which are now random variables, we obtain the respective reconstruction errors as

$$\varepsilon_L^2(N) = A_L K_{ff}(0, 0) - \sum_{m=0}^{N} \sum_{n=0}^{m} \frac{(2m - 2n + 1)(2n + 1)}{4} \cdot \int_{\zeta_L} K_{ff}(x, y, u, v) \, P_{m-n}(x) \cdot P_{m-n}(u) \, P_n(y) \, P_n(v) \, d\zeta_L \tag{5.13}$$

and

$$\varepsilon_Z^2(N) = A_Z K_{ff}(0, 0) - \sum_{n=0}^{N} \sum_{\substack{l \\ n - |l| = \text{even} \\ |l| \le n}} \frac{n + 1}{\pi} \cdot \int_{\zeta_Z} K_{ff}(x, y, u, v) \cdot [V_{nl}(x, y)]^* V_{nl}(u, v) \, d\zeta_Z \tag{5.14}$$

where $A_L = 4$ and $A_Z = \pi$, ζ_L is over the region $[-1 \le x, y, u, v \le 1]$ and ζ_Z is over the region $[x^2 + y^2 \le 1, u^2 + v^2 \le 1]$. Again, in the case of pseudo-Zernike moments, the reconstruction error is given by (5.14) with the condition $n - |l| =$ even eliminated, and $\{V_{nl}(x, y)\}$ is now the pseudo-Zernike polynomials as defined in Section II-D.

For a given value of N, both the normalized mean-square reconstruction errors $\varepsilon_L^2(N)/[A_L K_{ff}(0, 0)]$ and

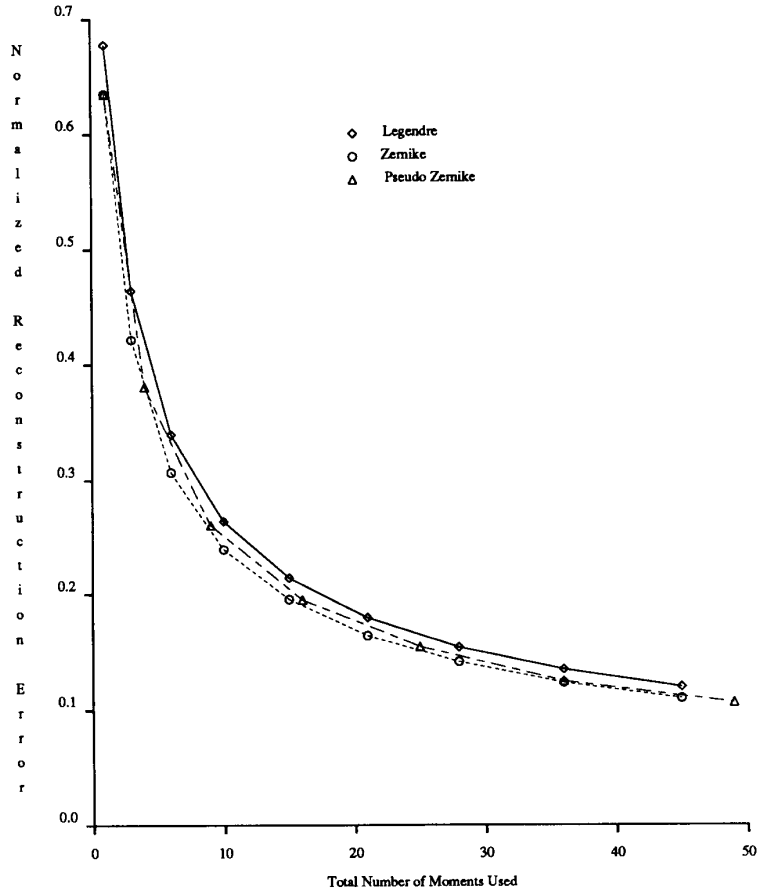

Fig. 4. Normalized reconstruction error for the case of homogeneous random fields ($c_1 = c_2 = 1$) (lines connecting data points are for illustration purposes).

$\varepsilon_Z^2(N)/[A_Z K_{ff}(0, 0)]$ depend on c_1 and c_2 only. They are shown in Fig. 4 for the case of $c_1 = c_2 = 1$. The results show that the mean-square reconstruction error of an image function can be reduced to a relatively small value by including enough higher order moments. The moment sets $\{\lambda_{mn}\}$ and $\{A_{nl}\}$ can also be interpreted as samples of the image function, and the reconstruction errors as the sampling errors. From Fig. 4, it is clear that the sampling technique using Zernike polynomials or pseudo-Zernike polynomials as basis functions is more efficient than that using Legendre polynomials as basis functions.

C. Reconstruction Error of Noisy Images

When the image function is corrupted by noise, moments of the noisy image are expected to be erroneous, generating large mean-square reconstruction error. Since higher order moments are more sensitive to noise, as demonstrated in Section III, it is easy to see that at a certain noise level, the image is best reconstructed by using moments of up to a certain optimal order. Using moments of orders higher than the optimal order in the reconstruction will degrade the reconstructed image quality because of the large amount of noise contained in the higher order moments.

For the purpose of illustration, we assume that the homogeneous random field $\boldsymbol{f}(x, y)$ is corrupted by zero-mean additive white noise which is uncorrelated to $\boldsymbol{f}(x, y)$:

$$E\{\boldsymbol{f}(x, y)\,\boldsymbol{n}(x, y)\} = E\{\boldsymbol{f}(x, y)\}\,E\{\boldsymbol{n}(x, y)\} = 0. \tag{5.15}$$

It is shown in the Appendix that under this condition, the noisy reconstruction error, when moments of orders $\leq N$ are used, is given by

$$\xi^2(N) = \varepsilon^2(N) + N_{\text{total}}\,\sigma_n^2 \tag{5.16}$$

where σ_n^2 is the noise variance and $\varepsilon^2(N)$ is the reconstruction error under noise-free conditions, which is given by (5.13) for Legendre moments and (5.14) for Zernike moments and pseudo-Zernike moments (with the condition $n - |l| =$ even eliminated and $\{V_{nl}(x, y)\}$ defined as pseudo-Zernike polynomials). The term N_{total}, which is the total number of independent moments of order $\leq N$ used for the reconstruction, is given by (5.7) for the cases

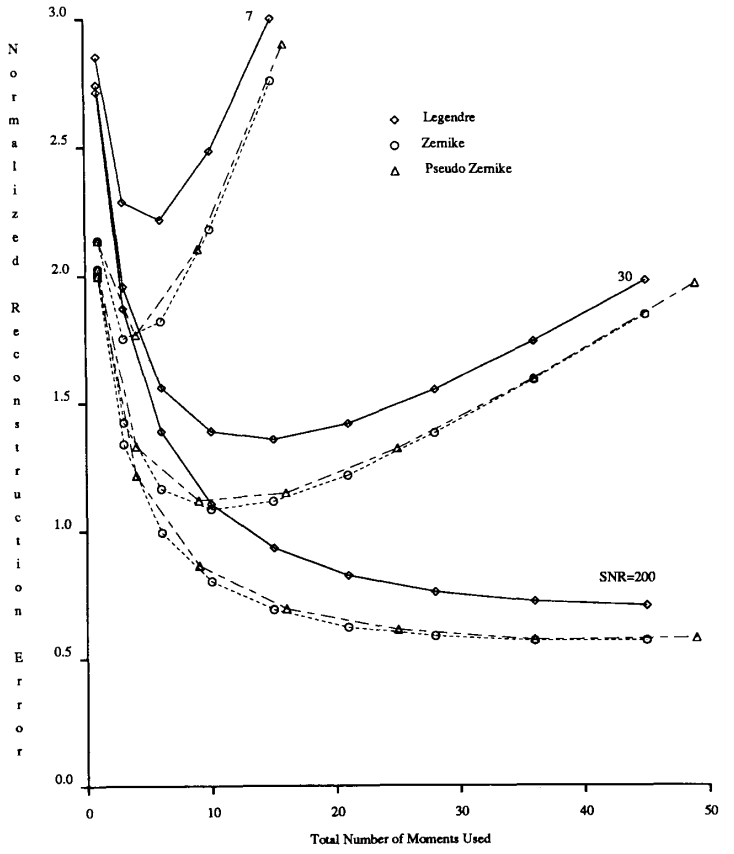

Fig. 5. Normalized reconstruction error for the case of homogeneous random fields with uncorrelated additive white noise ($c_1 = c_2 = 1$) (lines connecting data points are for illustration purposes).

of Legendre and Zernike moments and by (5.8) for the case of pseudo-Zernike moments. It follows that the additional error term due to the additive noise, which is the last term in (5.16), is the same for both Legendre and Zernike moments. If we normalized (5.16) throughout by $K_{ff}(0, 0)$, the average energy per unit area of the random field, we get the normalized reconstruction error as

$$\bar{\xi}^2(N) = \frac{\varepsilon^2(N)}{K_{ff}(0, 0)} + \frac{N_{\text{total}}}{\text{SNR}} \tag{5.17}$$

where SNR is the signal-to-noise ratio defined as

$$\text{SNR} = \frac{K_{ff}(0, 0)}{\sigma_n^2}. \tag{5.18}$$

For a deterministic image function $f(x, y)$, the normalized reconstruction error becomes

$$\bar{\xi}^2(N) = \frac{e^2(N)}{\frac{1}{A}\iint_{\zeta} [f(x, y)]^2 \, dx \, dy} + \frac{N_{\text{total}}}{\text{SNR}} \tag{5.19}$$

where the signal-to-noise ratio is now defined as the ratio of the image energy per unit area to the noise variance:

$$\text{SNR} = \frac{\frac{1}{A}\iint_{\zeta} [f(x, y)]^2 \, dx \, dy}{\sigma_n^2} \tag{5.20}$$

with A the area of the region ζ. The term $e^2(N)$ is the reconstruction error under noise-free conditions and is given by (5.5) and (5.6) for Legendre and Zernike moments, respectively.

The normalized reconstruction error as defined in (5.17) for the case of homogeneous random fields is plotted in Fig. 5 and summarized in Table III for SNR = 7, 30, 200. It is clear from the results that the optimum number of moments which are useful to the reconstruction process depends on the noise level added. For an SNR of 30, Legendre moments of order as high as 4, which amounts to 15 moments, should be used. Using Legendre moments higher than order 4 will, instead of improving the reconstruction, degrade the quality of the reconstructed image.

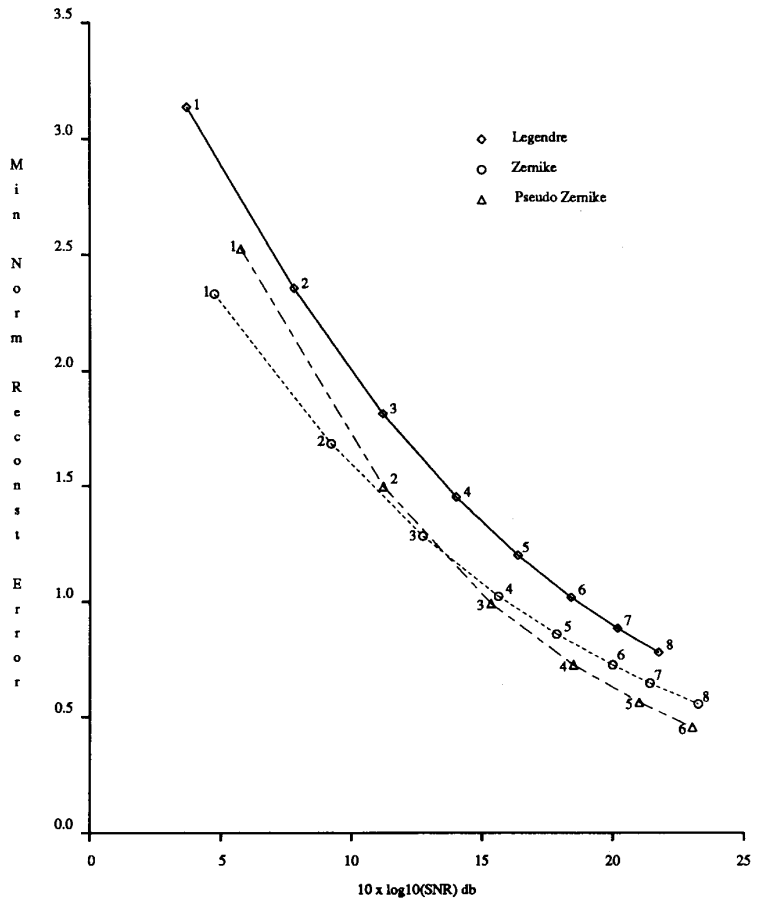

Fig. 6. Minimum normalized reconstruction error versus SNR in dB ($c_1 = c_2 = 1$). The numbers on the curves are the highest orders of moments which still remain useful for reconstruction (lines connecting data points are for illustration purposes).

TABLE III
NORMALIZED RECONSTRUCTION ERROR FOR THE CASE OF HOMOGENEOUS RANDOM FIELDS WITH UNCORRELATED ADDITIVE WHITE NOISE ($c_1 = c_2 = 1$)

SNR	Type of Moment		Optimal Order of Moment N	Total Number of Moments N_{total}	Normalized Reconstruction Error $\xi^2(N)$
7	LM	λ_{mn}	2	6	2.22
	ZM	A_{nl}	1	3	1.75
	PM	A_{nl}	1	4	1.77
30	LM	λ_{mn}	4	15	1.36
	ZM	A_{nl}	3	10	1.08
	PM	A_{nl}	2	9	1.12
200	LM	λ_{mn}	8	45	0.70
	ZM	A_{nl}	7	36	0.57
	PM	A_{nl}	5	36	0.57

In general, the normalized reconstruction error for noisy images reaches a minimum value and then starts to increase as the number of moments increases. Fig. 6 shows the minimum normalized reconstruction error (and hence the optimum order of moments) as a function of SNR, and Table IV shows a summary. From the plot, it is possible to estimate how much noise can be tolerated if moments of up to certain orders are to be used.

D. Experimental Results

Fig. 7 shows examples of the reconstruction of a binary-value letter E from its Legendre, Zernike, and pseudo-Zernike moments by including increasingly higher order moments. The image array size is 64 × 64. It illustrates the fact that a relatively small finite set of moments may characterize an image adequately, but the fine detail can be recreated only by including higher order moments. The normalized reconstruction errors as defined in (5.4) are computed and shown in Fig. 8.

Next, white Gaussian noise with variances 1.0 and 0.125 is generated and added to the original letter E. The signal-to-noise ratios are 224 and 1792 for the case of Legendre moments, and 284 and 2274 for the cases of Zernike and pseudo-Zernike moments. The reconstructed letters are shown in Fig. 9, and the corresponding normalized reconstruction errors as defined in (5.19) are computed and shown in Fig. 10. The results show that higher order moments are less reliable because the added noise results in degradation of the reconstructed image.

TABLE IV
MINIMUM NORMALIZED RECONSTRUCTION ERROR AND THE OPTIMUM ORDER OF MOMENTS AS A FUNCTION OF SNR IN dB FOR THE CASE OF HOMOGENEOUS RANDOM FIELDS ($c_1 = c_2 = 1$)

Type of Moment		$10 \times \log_{10}$ SNR dB	Minimum Normalized Reconstruction Error $\xi^2(N)$	Optimal Order of Moment N
LM	λ_{mn}	3.70	3.14	1
		7.80	2.36	2
		11.19	1.82	3
		14.00	1.45	4
		16.36	1.20	5
		18.39	1.02	6
		20.17	0.89	7
		21.74	0.78	8
ZM	A_{nl}	4.74	2.33	1
		9.21	1.68	2
		12.72	1.28	3
		15.62	1.02	4
		17.85	0.86	5
		19.98	0.73	6
		21.41	0.65	7
		23.25	0.56	8
PM	A_{nl}	5.75	2.53	1
		11.21	1.50	2
		15.33	0.99	3
		18.49	0.73	4
		21.00	0.56	5
		23.03	0.46	6

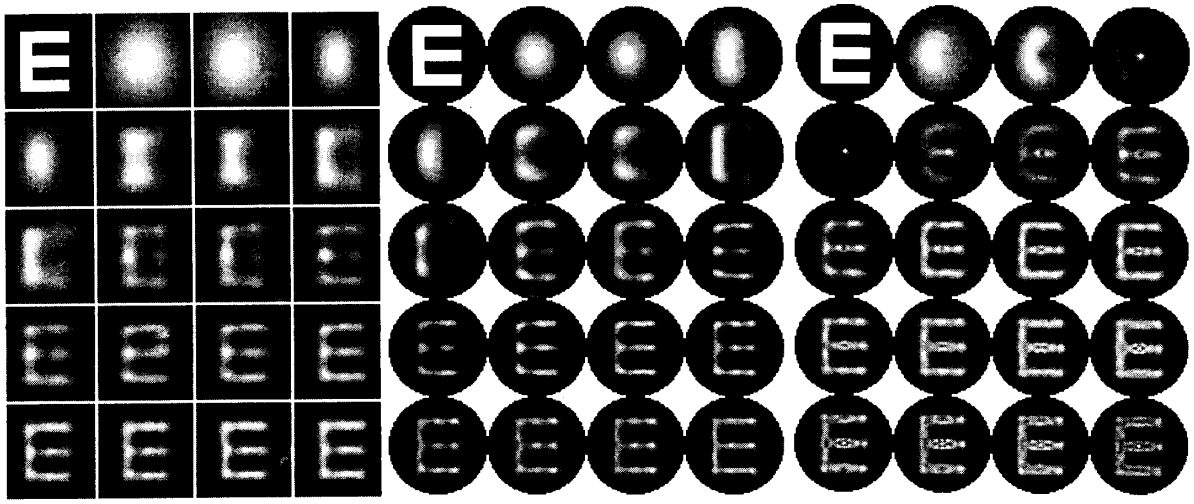

(a) (b) (c)

Fig. 7. (a) Reconstruction of the letter E by Legendre moments. From top row to bottom row and left to right in each row: original input image, reconstructed image with up to second-order moment (a total of six moments) through up to 20th-order moment (a total of 231 moments). (b) Reconstruction of the letter E by Zernike moments. From top row to bottom row and left to right in each row: original input image, reconstructed image with up to second-order moment (a total of six moments) through up to 20th-order moment (a total of 231 moments). (c) Reconstruction of the letter E by pseudo-Zernike moments. From top row to bottom row and left to right in each row: original input image, reconstructed image with up to second-order moment (a total of nine moments) through up to 20th-order moment (a total of 441 moments).

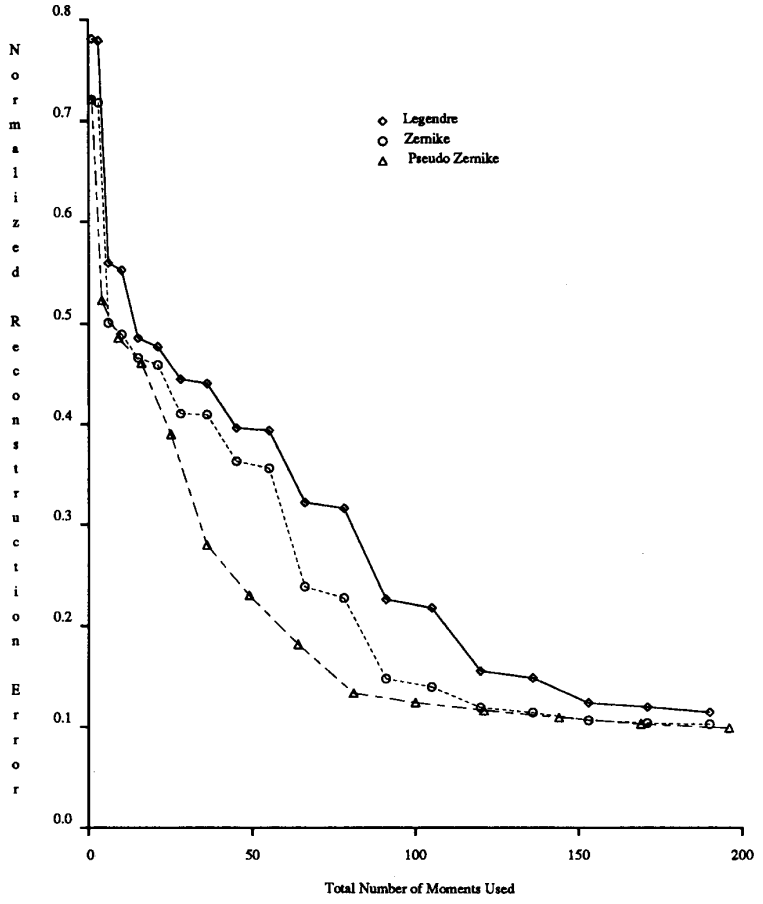

Fig. 8. Normalized reconstruction error of the letter "E" (lines connecting data points are for illustration purposes).

VI. Conclusion

Various moments, including geometric, Legendre, Zernike, pseudo-Zernike, rotational, and complex moments, are examined and compared. Three fundamental issues related to their usefulness in image analysis are addressed. They include 1) sensitivity to image noise, 2) aspects of information redundancy, and 3) capability for image representation. Both analytic characterization and experimental results of the investigation are presented.

From the noise analysis, we first show that higher order moments are more vulnerable to noise, and then we determine the number of coefficients (and hence the set of moments up to a certain order) for optimal image representation under a given noisy condition. We also show that the orthogonal moments (i.e., Legendre, Zernike, and pseudo-Zernike) are better than the other types of moments in terms of information redundancy. In terms of overall performance, Zernike and pseudo-Zernike moments outperform the others.

However, we should point out that the criterion of mean-square reconstruction error applies only to the case of additive random noise and does not apply to contextual or signal-dependent noise. For example, the letter E can be easily changed into an 8 by alteration of a few pixels. This will not change the mean-square reconstruction error measurement much, but will change the context of the image substantially. In fact, if the noise level is too high, one might want to first segment the original image and then extract moments from the segmented image instead of the entire scene.

Appendix
Derivation of Noisy Reconstruction Error

We consider only the case of Legendre moments here. The derivation for the cases of Zernike and pseudo-Zernike moments follows similarly. Let λ_{mn} and κ_{mn} be the Legendre moments of the random field $f(x, y)$ and the additive noise process $n(x, y)$, respectively; then the Legendre moments of the noise corrupted random field are

$$\Lambda_{mn} = \lambda_{mn} + \kappa_{mn} \tag{A.1}$$

where

$$\lambda_{mn} = \frac{(2m + 1)(2n + 1)}{4} \cdot \int_{-1}^{1} \int_{-1}^{1} f(x, y)\, P_m(x)\, P_n(y)\, dx\, dy \tag{A.2}$$

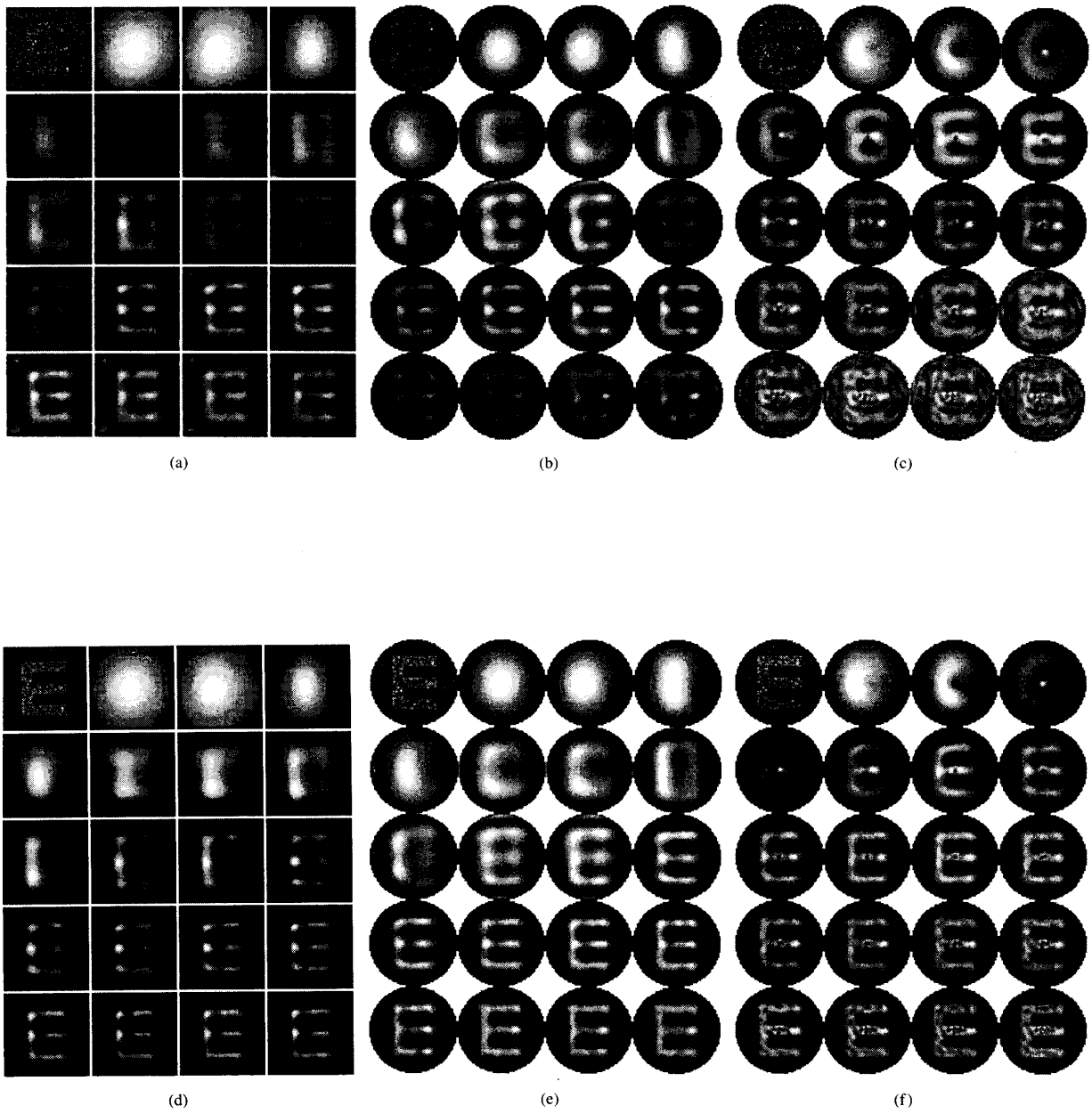

Fig. 9. (a) Reconstruction of the letter E by Legendre moments with white Gaussian noise of variance 1.0 added. From top row to bottom row and left to right in each row; noisy input image, reconstructed image with up to second-order (a total of six moments) through up to 20th-order moment (a total of 231 moments). (b) Reconstruction of the letter E by Zernike moments with white Gaussian noise of variance 1.0 added. From top row to bottom row and left to right in each row; noisy input image, reconstructed image with up to second-order (a total of six moments) through up to 20th-order moment (a total of 231 moments). (c) Reconstruction of the letter E by pseudo-Zernike moments with white Gaussian noise of variance 1.0 added. From top row to bottom row and left to right in each row; noisy input image, reconstructed image with up to second-order (a total of the nine moments) through up to 20th-order moment (a total of 441 moments). (d) Reconstruction of the letter E by Legendre moments with white Gaussian noise of variance 0.125 added. From top row to bottom row and left to right in each row; noisy input image, reconstruted image with up to second-order (a total of six moments) through up to 20th-order moment (a total of 231 moments). (e) Reconstructin of the letter E by Zernike moments with white Gaussian noise of variane 0.125 added. From top row to bottom row and left to right in each row; noisy input image, reconstructed image with up to second-order (a total of six moments) through up to 20th-order moment (a total of 231 moments). (f) Reconstruction of the letter E by pseudo-Zernike moments with white Gaussian noise of variance 0.125 added. From top row to bottom row and left to right in each row; noisy input image, reconstructed image with up to seond-order (a total of nine moments) through up to 20th-order moment (a total of 441 moments).

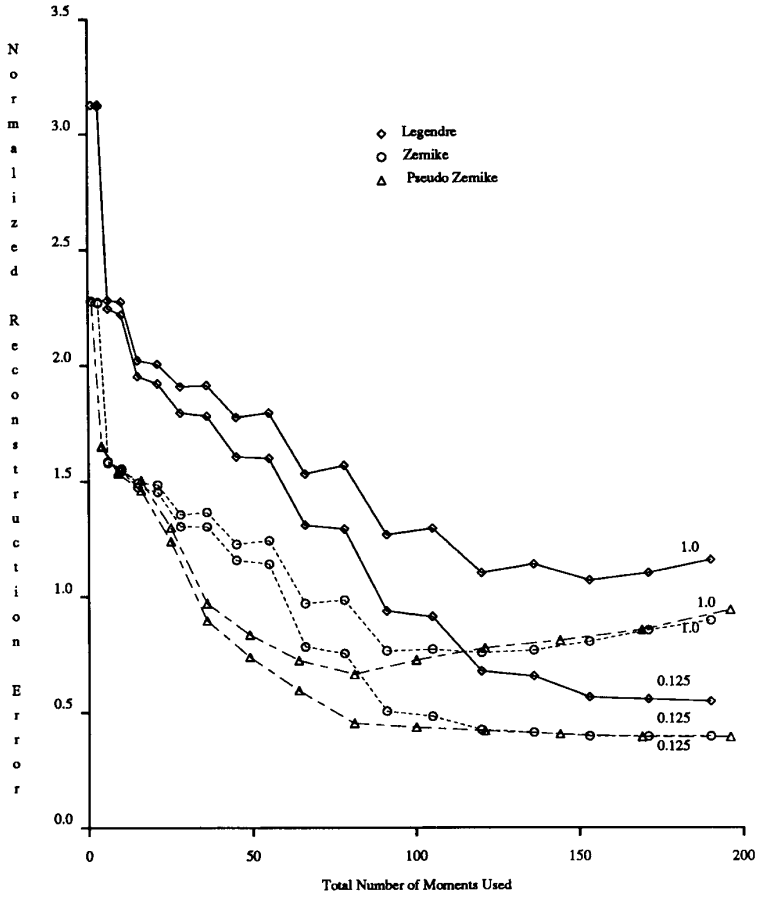

Fig. 10. Normalized reconstruction error of the letter "E" with additive white Gaussian noise (lines connecting data points are for illustration purposes).

and

$$\kappa_{mn} = \frac{(2m+1)(2n+1)}{4} \cdot \int_{-1}^{1}\int_{-1}^{1} \boldsymbol{n}(x, y)\, P_m(x)\, P_n(y)\, dx\, dy. \quad \text{(A.3)}$$

The reconstructed version of $\boldsymbol{f}(x, y)$ based on the noisy Legendre moments of order $\leq N$ is

$$\hat{\boldsymbol{f}}(x, y) = \sum_{m=0}^{N}\sum_{n=0}^{m} \Lambda_{mn} P_m(x)\, P_n(y). \quad \text{(A.4)}$$

The noisy mean-square reconstruction error is defined as

$$\begin{aligned}\xi^2(N) &= E\left\{\int_{-1}^{1}\int_{-1}^{1} \left[\boldsymbol{f}(x, y) - \hat{\boldsymbol{f}}(x, y)\right]^2 dx\, dy\right\} \\ &= E\left\{\int_{-1}^{1}\int_{-1}^{1} \left[\boldsymbol{f}(x, y)\right]^2 dx\, dy\right\} \\ &\quad - 2E\left\{\int_{-1}^{1}\int_{-1}^{1} \left[\boldsymbol{f}(x, y)\hat{\boldsymbol{f}}(x, y)\right] dx\, dy\right\} \\ &\quad + E\left\{\int_{-1}^{1}\int_{-1}^{1} \left[\hat{\boldsymbol{f}}(x, y)\right]^2 dx\, dy\right\}. \quad \text{(A.5)}\end{aligned}$$

The first term is easily evaluated to be $A_L K_{ff}(0, 0)$ where A_L is the area of the integration region and $K_{ff}(0, 0)$ is the average energy of the random field $\boldsymbol{f}(x, y)$ as defined in (3.3). Using (A.1)–(A.4) and the assumptions that $\boldsymbol{f}(x, y)$ and $\boldsymbol{n}(x, y)$ are both of zero mean and uncorrelated, the last two terms are evaluated to be

$$\begin{aligned}&\sum_{m=0}^{N}\sum_{n=0}^{m} \frac{(2m-2n+1)(2n+1)}{4} \\ &\quad \cdot \int_{-1}^{1}\int_{-1}^{1}\int_{-1}^{1}\int_{-1}^{1} \left[K_{ff}(x, y, u, v) + K_{nn}(x, y, u, v)\right] \\ &\quad \cdot P_{m-n}(x)\, P_{m-n}(u)\, P_n(y)\, P_n(v)\, dx\, dy\, du\, dv. \quad \text{(A.6)}\end{aligned}$$

Substituting (3.4) into the above and using the orthogonal property of the Legendre polynomials, the noisy reconstruction error becomes

$$\xi^2(N) = \varepsilon_L^2 + N_{\text{total}}\sigma_n^2 \quad \text{(A.7)}$$

where ε_L^2 is the noiseless reconstruction error as defined in (5.13) and

$$N_{\text{total}} = \sum_{m=0}^{N} \sum_{n=0}^{m} (1) = \frac{(N+1)(N+2)}{2} \quad \text{(A.8)}$$

is the total number of independent Legendre moments of order $\leq N$.

List of Symbols

GM	Geometric moments.
LM	Legendre moments.
ZM	Zernike moments.
PM	Pseudo-Zernike moments.
RM	Rotational moments.
CM	Complex moments.
M_{pq}	Geometric moments of order $(p+q)$.
λ_{mn}	Legendre moments of order $(m+n)$.
A_{nl}	Zernike moments of order n with repetition l.
D_{nl}	Rotational moments of order n with repetition l.
C_{pq}	Complex moments of order $(p+q)$.
$P_n(\cdot)$	nth-order Legendre polynomial.
a_{nj}	Coefficients of the nth-order Legendre polynomial.
$V_{nl}(\cdot)$	Zernike polynomials of order n with repetition l.
$R_{nl}(\cdot)$	Radial polynomials, real part of Zernike polynomials.
B_{nlk}	Coefficients of the radial polynomials of Zernike polynomials.
S_{nlk}	Coefficients of the radial polynomials of pseudo-Zernike polynomials.
$f(x, y)$	Deterministic real image intensity function.
$f(i, j)$	Discrete version of $f(x, y)$.
$\hat{f}(x, y)$	Reconstructed version of $f(x, y)$.
$\hat{f}(i, j)$	Discrete version of $\hat{f}(x, y)$.
$\boldsymbol{f}(x, y)$	Real homogeneous random field.
$\hat{\boldsymbol{f}}(x, y)$	Reconstructed version of $\boldsymbol{f}(x, y)$.
$\boldsymbol{n}(x, y)$	White noise process.
ζ	Region of $\boldsymbol{f}(x, y)$ over the xy plane.
ζ_L	Region $[-1 \leq x, y, u, v \leq 1]$.
ζ_Z	Region $[x^2 + y^2 \leq 1, u^2 + v^2 \leq 1]$.
A	Area of ζ.
$K_{ff}(\cdot, \cdot)$	Autocorrelation function of $\boldsymbol{f}(x, y)$.
$K_{nn}(\cdot, \cdot)$	Autocorrelation function of $\boldsymbol{n}(x, y)$.
$K_{ff}(0, 0)$	Average energy of $\boldsymbol{f}(x, y)$.
c_1, c_2	Correlation coefficients of $K_{ff}(\cdot, \cdot)$ in the x and y directions.
σ_n^2	Two-dimensional spectral density of $\boldsymbol{n}(x, y)$.
$\delta(\cdot, \cdot)$	Two-dimensional Delta function.
$\phi_{pq}(\cdot, \cdot)$	Moment weighting kernel.
$\boldsymbol{\Phi}_{pq}$	General moments of order $(p+q)$ of $\boldsymbol{f}(x, y)$.
$\boldsymbol{N}_{pq}$	General moments of order $(p+q)$ of $\boldsymbol{n}(x, y)$.
$\text{cov}\{\boldsymbol{N}_{pq}, \boldsymbol{N}_{rs}\}$	Covariance of $\boldsymbol{N}_{pq}$ and $\boldsymbol{N}_{rs}$.
SNR_{pq}	Unnormalized signal-to-noise ratios of order (p, q).
$\overline{\text{SNR}}_{pq}$	Normalized signal-to-noise ratios of order (p, q).
$\gamma(\cdot)$	Information redundancy ratio.
N_{total}	Total number of moments of order $\leq N$.
$e^2(\cdot)$	Mean-square reconstruction error of $f(x, y)$.
$\bar{e}^2(\cdot)$	Normalized version of $e^2(\cdot)$.
$\boldsymbol{\varepsilon}^2(\cdot)$	Mean-square reconstruction error of $\boldsymbol{f}(x, y)$.
$\bar{\boldsymbol{\varepsilon}}^2(\cdot)$	Normalized version of $\boldsymbol{\varepsilon}^2(\cdot)$.
$\xi^2(\cdot)$	Noisy mean-square reconstruction error.
$\bar{\xi}^2(\cdot)$	Normalized version of $\xi^2(\cdot)$.

References

[1] M.-K. Hu, "Pattern recognition by moment invariants," *Proc. IRE*, vol. 49, p. 1428, Sept. 1961.

[2] ——, "Visual pattern recognition by moment invariants," *IRE Trans. Inform. Theory*, vol. IT-8, pp. 179–187, Feb. 1962.

[3] F. L. Alt, "Digital pattern recognition by moments," in *Optical Character Recognition*, G. L. Fischer *et al.*, Eds. Washington, DC: Spartan, 1962, pp. 153–179; also published in *J. Ass. Comput. Mach.*, vol. 9, pp. 240–258, Apr. 1962.

[4] K. Udagawa, J. Toriwaki, and K. Sugino, "Normalization and recognition of two-dimensional patterns with linear distortion by moments," *Electron. Commun. Japan*, vol. 47, no. 6, pp. 34–46, 1964.

[5] R. G. Casey, "Moment normalization of handprinted characters," *IBM J. Res. Develop.*, vol. 14, pp. 548–557, Sept. 1970.

[6] F. W. Smith and M. H. Wright, "Automatic ship photo interpretation by the method of moments," *IEEE Trans. Comput.*, vol. C-20, pp. 1089–1094, Sept. 1971.

[7] S. A. Dudani, K. J. Breeding, and R. B. McGhee, "Aircraft identification by moment invariants," *IEEE Trans. Comput.*, vol. C-26, pp. 39–46, Jan. 1977.

[8] S. S. Reddi, "Radial and angular moment invariants for image identification," *IEEE Trans. Pattern Anal. Machine Intell.*, vol. PAMI-3, pp. 240–242, Mar. 1981.

[9] F. A. Sadjadi and E. L. Hall, "Three-dimensional moment invariants," *IEEE Trans. Pattern Anal. Machine Intell.*, vol. PAMI-2, pp. 127–136, Mar. 1980.

[10] M. R. Teague, "Image analysis via the general theory of moments," *J. Opt. Soc. Amer.*, vol. 70, pp. 920–930, Aug. 1980.

[11] J. F. Boyce and W. J. Hossack, "Moment invariants for pattern recognition," *Pattern Recognition Lett.*, vol. 1, no. 5-6, pp. 451–456, July 1983.

[12] Y. S. Abu-Mostafa and D. Psaltis, "Recognitive aspects of moment invariants," *IEEE Trans. Pattern Anal. Machine Intell.*, vol. PAMI-6, pp. 698–706, Nov. 1984.

[13] ——, "Image normalization by complex moments," *IEEE Trans. Pattern Anal. Machine Intell.*, vol. PAMI-7, pp. 46–55, Jan. 1985.

[14] C.-H. Teh and R. T. Chin, "On digital approximation of moment invariants," *Comput. Vision, Graphics, Image Processing*, vol. 33, pp. 318–326, 1986.

[15] R. Courant and D. Hilbert, *Methods of Mathematical Physics, Vol. I.* New York: Interscience, 1953.

[16] M. Born and E. Wolf, *Principles of Optics.* New York: Pergamon, 1975.

[17] F. Zernike, *Physica*, vol. 1, p. 689, 1934.

[18] A. B. Bhatia and E. Wolf, *Proc. Camb. Phil. Soc.*, vol. 50, pp. 40–48, 1954.

[19] E. R. Kretzmer, "Statistics of television signals," *Bell Syst. Tech. J.*, pp. 751–763, July 1952.

[20] L. E. Franks, "A model for the random video process," *Bell Syst. Tech. J.*, pp. 609–630, Apr. 1966.

[21] T. S. Huang, "The subjective effect of two-dimensional pictorial noise," *IEEE Trans. Inform. Theory*, vol. IT-11, pp. 45–53, Jan. 1965.

Cho-Huak Teh (S'79) received the B.Eng. degree with honors in 1980 and the M.Eng. degree in 1982, both in electrical engineering, from the National University of Singapore.

From 1980 to 1982 he was a Senior Tutor at the National University of Singapore. He is currently working toward the Ph.D. degree in electrical engineering at the University of Wisconsin, Madison. His research interests include image processing, signal processing, pattern recognition, computer vision, and related applications.

Mr. Teh is a member of the Pattern Recognition Society and the British Pattern Recognition Association.

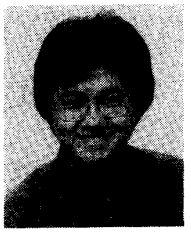

Roland T. Chin (S'75–M'79) received the B.S. degree with honors in 1975, the M.S. degree in 1976, and the Ph.D. degree in 1979, all in electrical engineering, from the University of Missouri, Columbia.

From 1979 to 1981 he was with Business and Technological Systems, Inc., MD, where he engaged in research in remote sensing data analysis and classification for NASA Goddard Space Flight Center, Greenbelt, MD. Since 1981 he has been on the faculty of the Department of Electrical and Computer Engineering and the Department of Computer Sciences, University of Wisconsin, Madison, where he is currently Associate Professor. His current research interests include image restoration, texture analysis, shape descriptions, pattern recognition, visual inspection, object recognition, and related applications.

Dr. Chin is a member of Eta Kappa Nu and Tau Beta Pi, and he is the recipient of the First Presidential Young Investigator Award in 1984.